The electronic origin and vibrational levels of the first excited singlet state of isocyanic acid (HNCO)

H. Laine Berghout[a] and F. Fleming Crim
Department of Chemistry, University of Wisconsin-Madison, Madison, Wisconsin 53706

Mikhail Zyrianov and Hanna Reisler
Department of Chemistry, University of Southern California, Los Angeles, California 90089

(Received 6 October 1999; accepted 28 December 1999)

The combination of vibrationally mediated photofragment yield spectroscopy, which excites molecules prepared in single vibrational states, and multiphoton fluorescence spectroscopy, which excites molecules cooled in a supersonic expansion, provides detailed information on the energetics and vibrational structure of the first excited singlet state (S_1) of isocyanic acid (HNCO). Dissociation of molecules prepared in individual vibrational states by stimulated Raman excitation probes vibrational levels near the origin of the electronically excited state. Detection of fluorescence from dissociation products formed by multiphoton excitation through S_1 of molecules cooled in a supersonic expansion reveals the vibrational structure at higher energies. Both types of spectra show long, prominent progressions in the N–C–O bending vibration built on states with different amounts of N–C stretching excitation and H–N–C bending excitation. Analyzing the spectra locates the origin of the S_1 state at $32\,449 \pm 20\ \mathrm{cm}^{-1}$ and determines the harmonic vibrational frequencies of the N–C stretch ($\omega_3 = 1034 \pm 20\ \mathrm{cm}^{-1}$), the H–N–C bend ($\omega_4 = 1192 \pm 19\ \mathrm{cm}^{-1}$), and the N–C–O bend ($\omega_5 = 599 \pm 7\ \mathrm{cm}^{-1}$), values that are consistent with several *ab initio* calculations. The assigned spectra strongly suggest that the N–C stretching vibration is a promoting mode for internal conversion from S_1 to S_0. © *2000 American Institute of Physics.* [S0021-9606(00)00212-9]

I. INTRODUCTION

Isocyanic acid, the simplest of the isocyanates, is both fundamentally interesting and practically important.[1] There are several experimental and theoretical studies of its first excited singlet state but no direct determination of the electronic origin. One of the primary impediments to such a measurement is the large difference between the equilibrium geometries of the ground electronic state (S_0) and the first excited singlet state (S_1), which makes the Franck–Condon factor for transitions from the ground vibrational level of S_0 to low lying vibrational levels of S_1 very small. Initially preparing vibrational states that have better Franck–Condon factors for the subsequent electronic excitation permits direct excitation of otherwise inaccessible vibrational states near the origin of the excited state. Combining the results of such measurements with observations of transitions to higher levels from the vibrationless ground state of HNCO molecules cooled in a supersonic expansion allows detailed analysis of the vibronic spectrum. The spectra have clear progressions in three different vibrations in the excited state, and this analysis locates the electronic origin, assigns the vibrations, and identifies a promoting mode for internal conversion.

Isocyanic acid (HNCO) belongs to the class of sixteen valence electron molecules that includes HN_3, CO_2, OCS, and H_2CCO (ketene). The highest occupied orbital in the ground state is the nonbonding $2a''$ orbital, and promotion of an electron from that orbital to the antibonding $10a'$ orbital produces the first excited singlet electronic state.[2] A large set of theoretical and experimental studies of the ground state[3–15] find that the S_0 equilibrium structure has a nearly linear N–C–O moiety lying along the *a*-axis with the H atom off the axis but in the N–C–O plane. Woo and Liu first investigated the ultraviolet absorption spectrum of HNCO,[16] and Dixon and Kirby provided the most detailed study to date.[2] They observed four different vibrational progressions beginning around $35\,500\ \mathrm{cm}^{-1}$ that they attributed to the N–C–O bending vibration in the electronically excited state. Their analysis of the rotational contours showed that the molecule is planar in S_1 with a N–C–O bond angle of about 125° and a N–C bond that is about 0.2 Å longer than the ground state equilibrium value. The observed rotational contours also suggested that the $S_1 \leftarrow S_0$ transition moment lies along the *c* axis, consistent with promotion of an electron from the out-of-plane $2a''$ orbital in the A' ground electronic state to the in-plane $10a'$ orbital in the A'' excited state. The large changes in the N–C–O bond angle and the N–C bond length produce small Franck–Condon factors and, hence, weak transitions between the ground vibrational level of S_0 and low lying vibrational levels of S_1.

All of the rovibrational states of S_1 dissociate to yield either the spin allowed products $[\mathrm{NH}(a\,^1\Delta) + \mathrm{CO}(X\,^1\Sigma^+)$ and $\mathrm{H}(^2S) + \mathrm{NCO}(X\,^2\Pi)]$ or the spin-forbidden products $[\mathrm{NH}(X\,^3\Sigma^-) + \mathrm{CO}(X\,^1\Sigma^+)]$ depending on the total energy. Excitation at wavelengths longer than 260 nm produces only the spin-forbidden products that experiment[17] and theory[18] suggest come from radiationless decay of the initial state

[a]Present address: Los Alamos National Laboratory, MS C920, DX-2, Los Alamos, New Mexico 87545.

through the ground electronic state to the triplet state, $S_1 \rightarrow S_0 \rightarrow T_1$, on which the dissociation occurs. Because calculations show that there is only a small barrier to decomposition on T_1 and that its origin lies several thousand wave numbers below the S_1 origin, all of the excitation wavelengths we use (250 nm to 300 nm) yield NH($X\,^3\Sigma^-$) as at least one of the decomposition products. Detecting either the spin-forbidden triplet NH product or the spin-allowed NCO product is the key to the electronic spectroscopy we perform. The internal conversion that begins the decomposition to triplet products also creates a competition between the NH($X\,^3\Sigma^-$)+CO($X\,^1\Sigma^+$) channel and the H(^2S) +NCO($X\,^2\Pi$) channel near the threshold for the latter at 260 nm.[19] The linewidths in the NCO photofragment yield spectra appear to reflect primarily the $S_1 \rightarrow S_0$ internal conversion, and their variation with vibrational state suggests that certain modes selectively promote the internal conversion. Because the coupling between S_1 and S_0 is rather weak, the internal conversion takes a few picoseconds at the highest excitation energies we use.[20,21]

There are several recent theoretical studies of electronically excited states of HNCO. Schinke and co-workers have calculated a large portion of the S_1 surface with the goal of understanding the dissociation in the electronically excited state and have explored the surface in five dimensions, fixing only the out-of-plane torsional angle.[22,23] They found a barrier of about 8000 cm^{-1} to N–H bond fission and a much smaller barrier of about 550 cm^{-1} to N–C bond fission on S_1. Their calculation finds stable *cis* and *trans* isomers with the *trans* isomer lying about 1000 cm^{-1} lower in energy,[22] and they estimate that the zero-point of S_1 lies about 31 500 cm^{-1} above that of S_0.[23] Morokuma and co-workers have studied the stationary points on several excited state surfaces of HNCO.[18,24,25] They calculate barrier heights that are similar to those of Schinke and coworkers and find the zero-point level of the S_1 *trans*-minimum about 30 600 cm^{-1} above that of S_0.[18,25] In a recent study, Stanton optimized the *cis*- and *trans*-structures and used an extrapolation procedure to estimate an adiabatic $S_1 \leftarrow S_0$ excitation energy of 32 970 cm^{-1} for the *trans* isomer.[26] Our goal is to measure the energies of vibrations as near the origin as possible in order to determine the vibrational frequencies in the excited state and to estimate the energy of the zero-point level of S_1.

II. EXPERIMENTAL APPROACH

We use two complementary approaches, both illustrated in Fig. 1, to probe the vibrational structure of the S_1 state of isocyanic acid at low energies, and we use conventional photofragment spectroscopy to interrogate vibrations at higher energies. In *vibrationally mediated photofragment yield spectroscopy*, shown on the right-hand side of the figure, stimulated Raman excitation prepares vibrational states in S_0 that have good Franck–Condon factors for subsequent excitation to low lying vibrational levels in the electronically excited state. This approach relies on radiationless decay of S_1 to the triplet state T_1 and decomposition of HNCO to NH($X\,^3\Sigma^-$)+CO($X\,^1\Sigma^+$). We obtain the electronic spectrum in the region of the origin by scanning the wavelength λ_{elec} of the electronic excitation laser while monitoring the

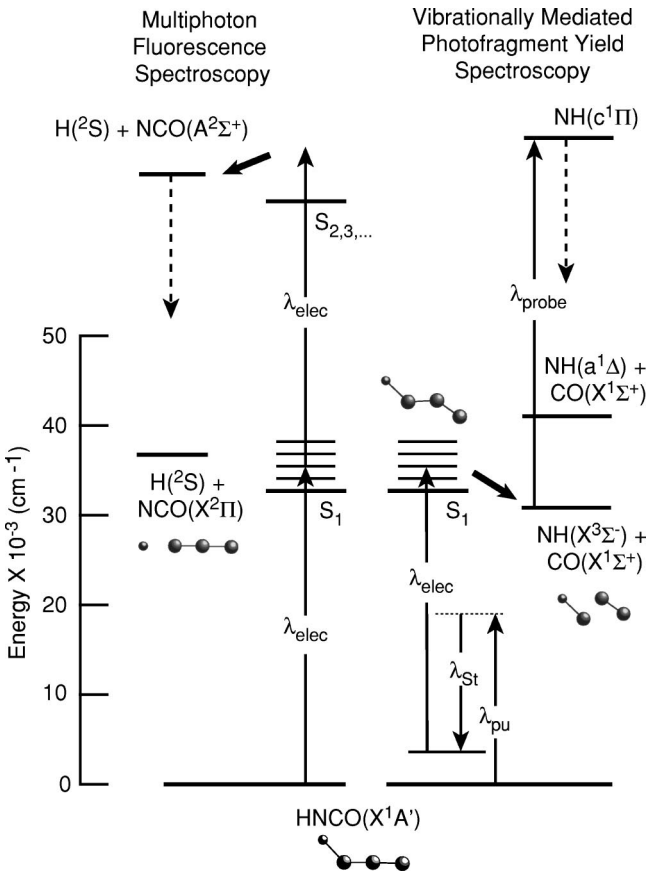

FIG. 1. Energy level diagram illustrating vibrationally mediated photofragment yield spectroscopy and multiphoton fluorescence spectroscopy of HNCO. The right-hand side of the figure shows vibrationally mediated photofragment yield spectroscopy in which stimulated Raman excitation prepares a vibrational state, a photon dissociates the vibrationally excited molecule, and laser induced fluorescence detects the triplet NH product. The left-hand side of the figure shows multiphoton fluorescence spectroscopy in which one photon excites HNCO to the S_1 state and another photon of the same wavelength promotes the molecule to a higher energy, dissociative state, forming electronically excited NCO whose fluorescence we detect.

NH($X\,^3\Sigma^-$) decomposition product by laser induced fluorescence (LIF). In *multiphoton fluorescence spectroscopy*, shown on the left-hand side of the figure, one photon with a wavelength λ_{elec} excites a transition to a low lying vibronic state in S_1, and a second photon from the same laser pulse carries the electronically excited molecule to a higher lying, dissociative electronic state in which HNCO decomposes to form H+NCO($A\,^2\Sigma^+$).[20] Monitoring the emission from the electronically excited NCO while varying the laser wavelength yields an electronic excitation spectrum of HNCO molecules cooled in a supersonic expansion.

The approach using stimulated Raman excitation for vibrational state preparation has the advantage of improving the Franck–Condon factor for transitions to states near the origin but has the disadvantages of exciting *Q*-branch transitions that lead to rotational congestion and of requiring that the system form the spin-forbidden product NH($X\,^3\Sigma^-$). The approach using electronic multiphoton excitation has the advantage of simplicity, since it requires only a single laser, and of exciting molecules from a cooled sample in which there is little rotational congestion, both of which make it

particularly useful for obtaining survey spectra extending to high excitation energies. However, it has the disadvantage that it relies on the Franck–Condon factor from the ground vibrational state and introduces the complication of multiphoton excitation to another electronic state. As the data below show, the two approaches together provide an excellent view of the vibronic states of HNCO up to 5500 cm^{-1} above the origin of S_1.

A. Electronic spectroscopy of selected vibrational states of HNCO

Stimulated Raman excitation (SRE) prepares molecules in the region of one quantum of N–H stretching excitation in HNCO. A 50 mJ, 6 ns pulse of 532 nm light from an injection seeded Nd^{3+}:YAG laser provides the pump wavelength (λ_{pu}) for the SRE process. The remaining 250 mJ of 532 nm light pumps a DCM dye laser to produce a 50 mJ pulse of 655 nm light at the Stokes wavelengths (λ_{St}) for SRE, as shown in Fig. 1. The focused pump and Stokes beams overlap spatially and temporally in the imaged region of a fluorescence cell, which also contains a microphone for obtaining photoacoustic Raman spectra to verify the excitation conditions. A 5 mJ pulse of ultraviolet light in the range of 28 500 cm^{-1} to 35 000 cm^{-1} from a frequency doubled dye laser excites the vibrationally prepared HNCO molecules from S_0 to S_1. The dye laser uses LDS 698, DCM, Sulforhodamine 640, Rhodamine 590, Rhodamine 610, and mixtures of those dyes. Directing a small amount of the electronic excitation light into a Fe/Ne hollow cathode lamp provides wavelength calibration via the optogalvanic effect.[27] Saturated laser induced fluorescence using 0.5 mJ of ultraviolet light from another frequency doubled dye laser detects the triplet NH fragment on the $R_1(3)$ rotational transition of the NH($A\,^3\Pi, v=0 \leftarrow X\,^3\Sigma^-, v=0$) band.[28–30] The delay between the vibrational excitation and electronic excitation pulses is 50 ns and that between the electronic excitation and probe pulses is 300 ns. Isocyanic acid slowly flows from a dry ice/acetone bath through the fluorescence cell in which its pressure is 150 mTorr. Both the vibrationally mediated photofragment spectroscopy experiments and the multiphoton fluorescence spectroscopy experiments use the reaction of phosphoric acid with potassium cyanate to produce HNCO, as described elsewhere.[31,32]

B. Electronic spectroscopy of ground vibrational states of HNCO

Several techniques provide low resolution $S_1 \leftarrow S_0$ spectra of the ground vibrational state of expansion-cooled HNCO. Multiphoton fluorescence spectroscopy works well in the region from 35 000 cm^{-1} to 38 500 cm^{-1} on which we primarily concentrate here, but photofragment yield spectroscopy of the NCO($X\,^2\Pi$) product gives good data in the higher energy region from 38 370 to 40 000 cm^{-1},[20] where rapid decay of the S_1 state competes effectively with two-photon excitation. In addition, photofragment yield spectroscopy of the NH($X\,^3\Sigma^-$) product permits observation of rotationally resolved bands in the region 35 000–37 200 cm^{-1}.[21] The spectra obtained using these methods are equivalent, as shown by their agreement in their common regions, and give reliable line positions even though they do not reflect the Franck–Condon factors for electronic excitation correctly.

The expansion consists of HNCO seeded in He or in a 30:70 He:Ne mixture at a typical total pressure of 1 atm. The carrier gas passes through a container of HNCO at −41 °C, at which temperature its pressure is about 15 Torr, and enters the chamber through a 0.5 mm diam pulsed nozzle. Analysis of several well-resolved bands yields a rotational temperature of 12 ± 3 K for HNCO in the free jet expansion. Either a single laser beam or counterpropagating pump and probe laser beams intersect the molecular beam 5–10 mm from the nozzle orifice. In the latter case, the delay between the laser pulses is 50 ns. Frequency doubled pulses having a 0.4 cm^{-1} bandwidth and 1–3 mJ of energy that come from an excimer laser pumped dye laser using Exciton dyes C540A, C500, and C480 excite HNCO in the expansion. A photomultiplier tube detects fluorescence collected by $f/1.5$ optics after it passes through filters. Observation of fluorescence from NCO, produced by resonant excitation through the S_1 state to a higher state in which dissociation forms electronically excited NCO($A\,^2\Sigma$),[33] as a function of wavelength yields the $S_1 \leftarrow S_0$ spectrum, a process illustrated in Fig. 1. In these experiments, we focus the 3 mJ laser pulse with a 50 cm focal length lens and monitor the fluorescence through glass filters that transmit light in the range 300–460 nm. The region between 36 400 and 36 500 cm^{-1} is inaccessible because it coincides with strong fluorescence from a HNCO state reached by two-photon excitation.[20,33] Additional higher energy data come from photofragment yield spectroscopy using laser induced fluorescence to detect either NH($X\,^3\Sigma^-$) or NCO($X\,^2\Pi_{3/2}$) products following one-photon electronic excitation, as described previously.[20,21]

III. RESULTS

The key to obtaining the vibrationally mediated photofragment yield spectra in the region of the origin of S_1 is the initial preparation of a vibrational level in the ground electronic state with nuclear motion that gives a good Franck–Condon factor for transitions near the origin and that has a specified amount of angular momentum about the *a* inertial axis. The vibrational character of different *a*-axis angular momentum states, designated by the quantum number K_a'', in the region of the fundamental N–H stretching vibration ν_1'' is remarkably varied.[34–36] Figure 2 is the room temperature stimulated Raman photoacoustic spectrum in the region of the N–H stretching fundamental with the assignments of Brown *et al.*[35,36] Stimulated Raman excitation for a near prolate top such as HNCO strongly favors $\Delta J = 0, \Delta K_a = 0$ transitions, and *Q*-branch transitions to each K_a'' level dominate the spectrum. We use the $(\nu_1''/\nu_x'')_{II} K_a'' = 2$ and $\nu_\beta'' K_a'' = 0$ transitions, marked with arrows in Fig. 2, to prepare the initial vibrational levels for photofragment yield spectroscopy. These transitions excite mixed vibrational states that contain bending excitation as well as stretching excitation. As indicated in the figure, the mixed states contain several quanta of excitation as different combinations of the H–N–C bend (ν_4''), the N–C–O bend (ν_5''), and torsion (ν_6''). One set of

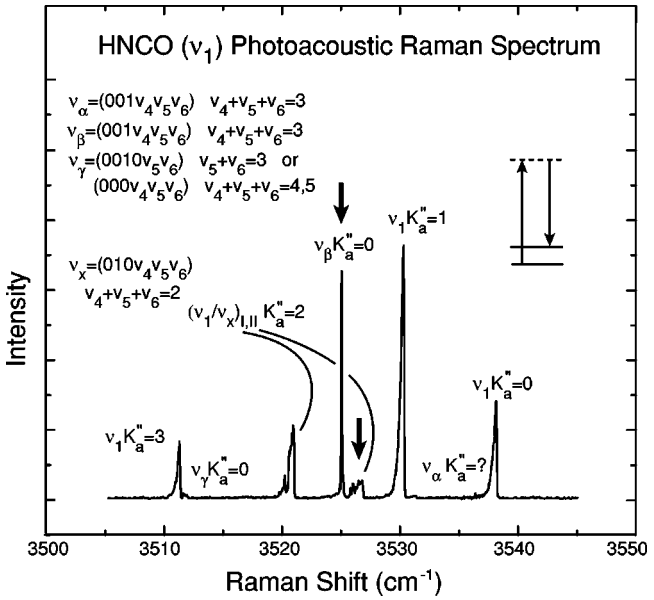

FIG. 2. Photoacoustic stimulated Raman excitation spectrum of HNCO in the region of the N–H stretching vibrations. The transitions reach states having different amounts of stretching and bending excitation. The arrows mark transitions used to prepare vibrationally excited molecules with a component of bending excitation.

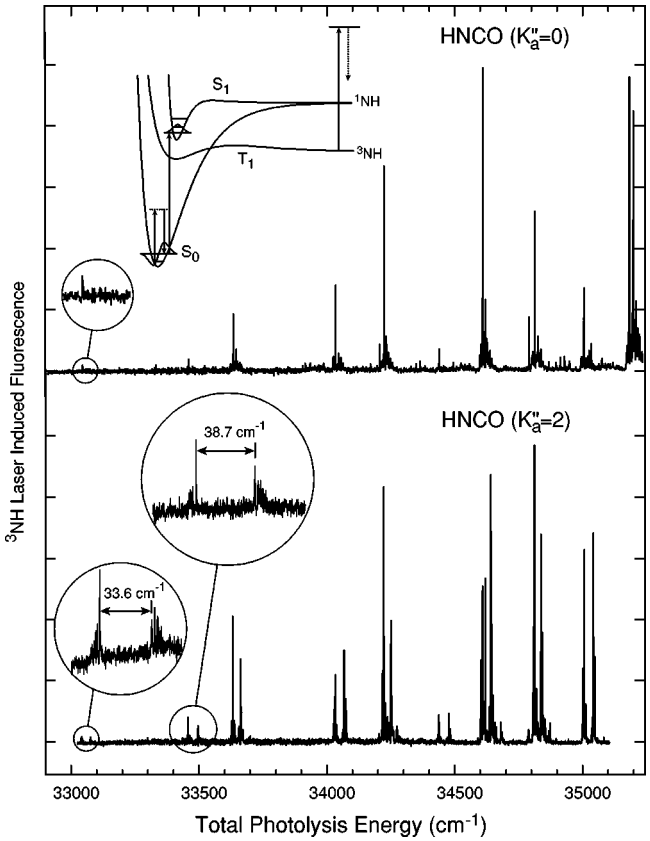

FIG. 3. Vibrationally mediated photofragment yield spectra for selected states of HNCO. The upper trace is for molecules initially prepared with no *a*-axis rotation ($K_a''=0$) that only reach a single excited state ($K_a'=1$). The lower trace is for molecules prepared with $K_a''=2$ and shows two transitions reaching $K_a'=1$ and $K_a'=3$. The separation of the pairs of transitions in the lower trace reflects the *a*-axis rotational constant for the electronically excited molecules.

experiments prepares the $(\nu_1''/\nu_x'')_{II}K_a''=2$ levels of HNCO by exciting the feature marked in the figure. The *Q*-branch excitation prepares a collection of rotational levels and allows us to observe limited rotational envelopes of the *P* and *R* branches of the photofragment yield spectrum from which we assign transitions and extract rotational constants. The $(\nu_1''/\nu_x'')_{II}K_a''=2$ vibrational level is a mixture that contains 21% of the N–H stretching vibration (ν_1'') and 79% of ν_x'', a combination state with one quantum of N–C–O antisymmetric stretch (ν_2'') and two quanta of bending excitation.[35,36]

The lower part of Fig. 3 is a vibrationally mediated photofragment yield spectrum from $(\nu_1''/\nu_x'')_{II}K_a''=2$ levels. The insets show the transitions to the two lowest lying vibrational levels of S_1 that we observe. Because the $S_1 \leftarrow S_0$ transition moment lies along the *c* axis of HNCO,[2] transitions with $\Delta K_a=\pm 1$ dominate.[37] We prepare an initial vibrational level with $K_a''=2$ and observe transitions to rovibrational levels of S_1 with $K_a'=1$ and 3. The transitions have their usual symmetric top labels of ${}^{\Delta K}\Delta J_{K''}(J'')$, and the most intense $K_a'=1$ and 3 features are ${}^PQ_2$ and ${}^RQ_2$ transitions, respectively. The *P*- and *R*-branch structure associated with each K_a band permits an estimate of the average *b*- and *c*-axis rotational constants B'. This value and the energy difference between ${}^PQ_2$ and ${}^RQ_2$ transitions provide an estimate, in the absence of K_a' specific vibrational state mixing and centrifugal distortion effects, of the A' rotational constant and, hence, the vibronic energy of the rotationless state, $E_{v'}$. A nonlinear least-squares fit of the rotational structure in the lowest energy features shows that the vibration in the excited electronic state lies $33\,039.2\pm0.2$ cm^{-1} above the vibrationless ground electronic state, where the uncertainty is one standard deviation of the fit. The spectrum is relatively uncongested up to 35 000 cm^{-1} with clear progressions of about 600 cm^{-1} and 1000 cm^{-1} that are likely to involve the two lowest energy vibrations of a' symmetry in S_1. As the figure shows, the separations of the ${}^PQ_2$ and ${}^RQ_2$ transitions differ significantly for the two vibrational states, being 33.6 cm^{-1} and 38.7 cm^{-1}, respectively. The A' rotational constant, which determines the spacing between the two *Q*-branch transitions, is different for the two excited state vibrations because they sample different geometries.

The second vibrationally mediated photofragment yield experiment uses SRE to prepare the $\nu_\beta'' K_a''=0$ levels of HNCO. The upper part of Fig. 3 is a vibrationally mediated photofragment yield spectrum from the $\nu_\beta K_a''=0$ vibrational level, which is a mixture of 10% ν_1'' and 90% ν_β'', where ν_β'' is the combination of one quantum of N–C–O symmetric stretch (ν_3'') and three quanta of bending excitation.[35,36] The spectrum has single *Q*-branch features since the only possible transitions from $K_a''=0$ are to states with $K_a'=1$. The ${}^RQ_0$ transitions (from $K_a''=0$) and ${}^PQ_2$ transitions (from $K_a''=2$) access the same levels of S_1 and appear at the same total energy in the two spectra.

Multiphoton fluorescence spectroscopy and conventional photofragment spectroscopy are less sensitive to transitions to the low lying vibrational levels of S_1 than vibrationally mediated photofragment yield spectroscopy. This decreased sensitivity to low vibrational levels of S_1 is probably due to

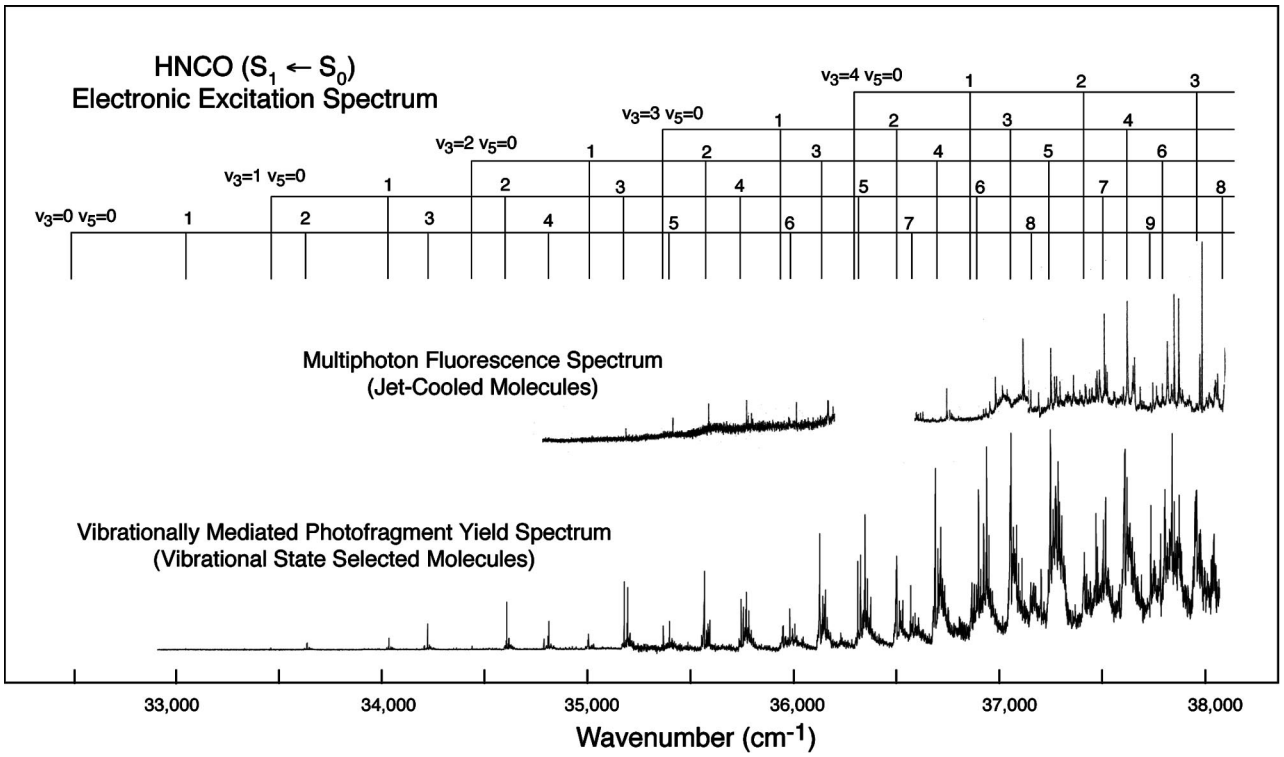

FIG. 4. Electronic excitation spectra for HNCO. The upper trace is the multiphoton fluorescence excitation spectrum for molecules cooled in a supersonic expansion. The lower trace is the vibrationally mediated photofragment yield excitation spectrum for molecules prepared in a selected vibrational state. The comb above the spectra shows the progressions in the N–C–O bending vibration (ν_5) built on different amounts of N–C stretching excitation (ν_3).

poorer Franck–Condon factors of the S_0 ground vibrational level compared with excited bending levels of S_0 for transitions to low lying vibrational levels of S_1. The upper trace in Fig. 4 is the spectrum of expansion-cooled HNCO, in which the transitions originate in the ground vibrational state of S_0. The portion of the spectrum from 35 000 to 38 500 cm^{-1} shown in the figure comes from multiphoton fluorescence spectroscopy. (Photofragment yield spectroscopy allows us to follow the same spectrum out to 40 000 cm^{-1}, as shown elsewhere.[20]) The lower trace in the figure is the vibrationally mediated photofragment yield spectrum from $K_a''=0$, and the comb above the spectra labels the stretching states and prominent progressions in the bending vibration that come from the analysis described below. Simulating the spectrum using transitions to three vibrations identifies many features and produces a consistent set of assignments. The vibrationally mediated photofragment yield spectrum in the lower trace becomes progressively more congested with increasing energy, but the multiphoton fluorescence spectrum, which originates in fewer initial J states, has sharp structure with all resolved bands showing c-type rotational structure. The two together allow us to unravel much of the vibrational structure of the S_1 state.

IV. ANALYSIS AND DISCUSSION

A. Simulation

Our approach to simulating the spectra and assigning the many transitions we observe to different vibrations in the first excited state of HNCO is to perform a detailed analysis of the lowest energy transitions, where the spectrum is relatively uncongested, and use those assignments as a guide to the higher energy region where the spectrum is more congested. Because the vibrational energy in the excited state ranges up to 5500 cm^{-1}, the spectrum is complicated, but we are able to identify and assign progressions in three vibrations systematically and consistently, albeit with less certainty at the highest energies.

The vibrationally mediated photofragment spectrum for $K_a''=2$, shown in Figs. 3 and 5, has distinct doublets corresponding to $\Delta K_a=\pm 1$ transitions. The different separations of the transitions suggest that they reach different vibrational states, and the spacing of the doublets helps us sort the transitions by vibrational state. With that clue, we can identify progressions in two vibrations of about 600 cm^{-1} and 1000 cm^{-1}. The two progressions appear to converge to a common origin near 32 450 cm^{-1}, located at an energy that is lower than the lowest energy transition we observe by one quantum of the lower frequency vibration. Figure 5 is a plot of the vibrationally mediated photofragment yield spectrum from the $(\nu_1''/\nu_x'')_{II}K_a''=2$ levels along with a simulation using three vibrations and the assumption that the progressions share a common vibrational level at 32 449 cm^{-1}. The simulation parameters (Table I) come from a two-step analysis of the low energy transitions. We determine the rotational constants (A' and B') and band origins (E_0+E_v') in Table II by a fit of the rotational contours of the individual bands in Fig. 5. A separate nonlinear least-squares fit of these band origins and rotational constants by the parameters for three anharmonic oscillators, as described below, gives the constants in

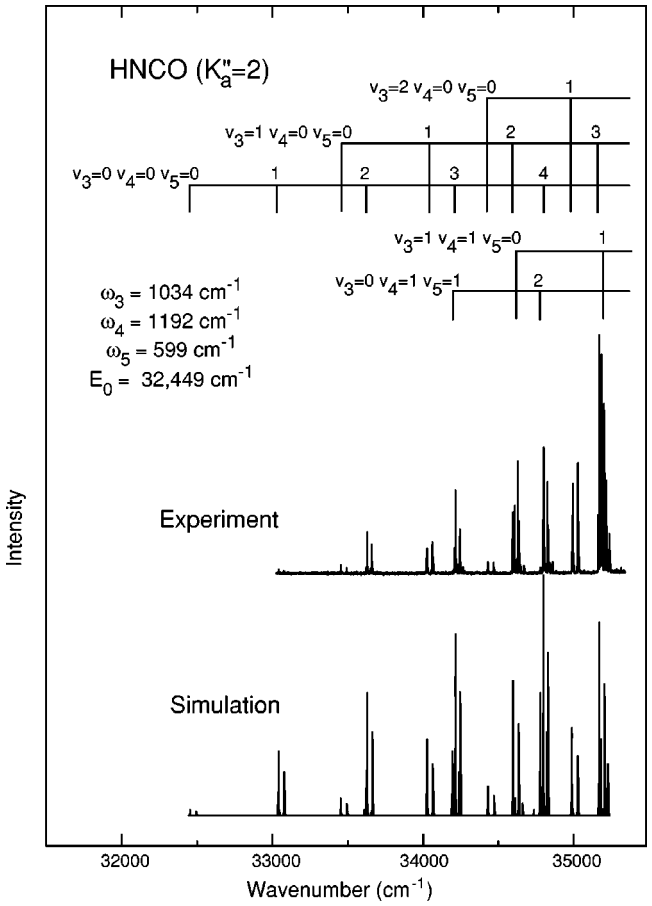

FIG. 5. Vibrationally mediated photofragment yield spectra, simulation, and assignments for transitions from selected states of HNCO. The upper trace is the measured photofragment yield spectrum from $K_a''=2$, and the lower trace is a simulation using three vibrations. The comb above the spectra shows the progressions in the N–C–O bending vibration (ν_5) built on different amounts of N–C stretching excitation (ν_3) and H–N–C bending excitation (ν_4).

TABLE I. Parameters for spectral simulation.

	Parameter	Value[a]
E_0	energy of common state	32 449± 20 cm^{-1}
ω_3	energy of N–C stretch vibration	1034± 11 cm^{-1}
ω_4	energy of H–N–C bending vibration	1192± 19 cm^{-1}
ω_5	energy of N–C–O bending vibration	599± 7 cm^{-1}
χ_{33}	N–C stretch anharmonicity	−11.6± 1.7 cm^{-1}
χ_{44}	H–N–C anharmonicity	−15.2± 5.0 cm^{-1}
χ_{55}	N–C–O anharmonicity	−0.2± 0.7 cm^{-1}
χ_{34}	off-diagonal anharmonicity	2.2± 5.1 cm^{-1}
χ_{35}	off-diagonal anharmonicity	−14.3± 2.2 cm^{-1}
χ_{45}	off-diagonal anharmonicity	−2.5± 3.5 cm^{-1}
A_e'	upper state A rotational constant	4.97± 0.40 cm^{-1}
α_3	rotation-vibration interaction constant of ν_3	−0.07± 0.12 cm^{-1}
α_4	rotation-vibration interaction constant of ν_4	−0.09± 0.21 cm^{-1}
α_5	rotation-vibration interaction constant of ν_5	0.29± 0.07 cm^{-1}
B'	upper state B rotational constant	0.375± 0.005 cm^{-1}
$E_{v''}+E_{Ka''}$	lower state energy	3645.3 cm^{-1}
B''	lower state B rotational constant[b]	0.365 cm^{-1}
K_a''	initial state K_a level	2
T	rotational temperature	15 K
$\Delta\nu$	laser bandwidth	0.25 cm^{-1}

[a]Uncertainties are one standard deviation of the least-squares fit.
[b]Ground state rotational constant from Ref. 34.

Table I. We simulate the spectrum using those constants and scaling the intensities of the transitions with the number of quanta in each mode.[40]

Extending the simulation to higher energies, as shown by the comb above the spectra in Fig. 4, assigns many of the transitions in the higher energy region. Because the N–C–O moiety bends and the N–C bond stretches upon electronic excitation, those two motions are likely to produce long progressions, suggesting that the two vibrations responsible for the prominent progressions at low energy are the N–C–O bend (ν_5) near 600 cm^{-1} and the N–C stretch (ν_3) near 1000 cm^{-1}. As the labels in Fig. 4 indicate, the bend appears with up to nine quanta of excitation and the stretch with at least four. Progressions in the N–C–O bend are the dominant feature of the electronic spectrum. The first member of each progression is weak, but the intensity grows with increasing bending excitation and goes through a maximum in the region of four to six quanta. At higher energies, other transitions, which also show progressions in the bending vibration, appear but are not explained by N–C stretching and N–C–O bending excitation alone.

Careful examination of the low energy region of the spectrum in Fig. 5 shows other progressions in the bend that are very weak but become prominent at higher energies. There is a progression beginning with a weak transition at 34 620 cm^{-1}, about 2170 cm^{-1} above the proposed origin, and extending to higher energies with increasing amounts of N–C–O bending excitation. We suspect that the first member of the progression located 2170 cm^{-1} above the origin is a combination ($\nu_3+\nu_4$) of the N–C stretch (ν_3) and the H–N–C bend (ν_4), an assignment that places the H–N–C bending wave number at about 1170 cm^{-1}. Closer inspection of the other low lying bands supports this assignment. Another, even weaker, progression of transitions in the 600 cm^{-1} N–C–O bend (ν_5), begins at 34 205 cm^{-1}, about 1755 cm^{-1} above the proposed origin. Assuming this transition is the second member ($\nu_4+\nu_5$) of a progression built on the H–N–C bend (ν_4), we estimate the wave number of the H–N–C bend to be about the same 1155 cm^{-1}, where we ignore the anharmonicity of the vibrations. (The combs in Fig. 5 mark both of these progressions.) Placing the H–N–C bend near 1160 cm^{-1} identifies several additional strong progressions in the N–C–O bend (ν_5) built on combinations of several quanta of N–C stretch ($v_3=0-4$) and several quanta of H–N–C bend ($v_4=0-2$). These progressions are particularly prominent in the spectrum of jetcooled molecules that extends to 40 000 cm^{-1}.[20]

Guided by our preliminary assignments, we fit the band origins in Table II to the expression for three anharmonic oscillators (in cm^{-1}),[37,38]

TABLE II. Energies and rotational constants for the simulation and experiment.[a]

			Experimental values				Calculated values					
v_3	v_4	v_5	$E(K'_a=1)$[b]	$E(K'_a=3)$[b]	A'[c]	B'[d]	$E_0+E'_v$	E'_v	E'_v	$\Delta E'_v$[e]	A'	$\Delta A'$[e]
0	0	1	33043.4	33077.0	4.57	0.369	33039.2	590.2	590.3	−0.1	4.62	−0.05
0	0	2	33633.2	33664.0	4.22	0.374	33629.4	1180.4	1180.1	0.3	4.33	−0.10
0	0	3	34223.0	34250.6	3.83	0.378	34219.6	1770.6	1769.5	1.1	4.04	−0.21
0	0	4	34812.1	34837.1	3.50	0.373	34809.0	2360.0	2358.5	1.5	3.75	−0.25
0	0	5	35401.5	35426.5	3.50	0.370	35398.4	2949.4	2947.1	2.3	3.46	0.04
1	0	0	33458.4	33497.1	5.20	0.370	33453.6	1004.6	1004.9	−0.3	4.98	0.23
1	0	1	34033.7	34068.3	4.70	0.374	34029.4	1580.4	1580.8	−0.4	4.69	0.01
1	0	2	34608.8	34641.5	4.46	0.372	34604.7	2155.7	2156.3	−0.5	4.40	0.06
1	0	3	35181.8	35213.3	4.31	0.372	35177.9	2728.9	2731.4	−2.5	4.11	0.20
2	0	0	34439.0	34477.8	5.22	0.371	34434.1	1985.1	1986.4	−1.3	5.05	0.18
2	0	1	35006.0	35040.5	4.68	0.370	35001.7	2552.7	2548.0	4.7	4.76	−0.08
3	0	0	35396.3	35434.2	5.11	0.370	35391.6	2942.6	2944.7	−2.2	5.12	−0.01
0	1	1	34204.6	34237.8	4.52	0.374	34200.5	1751.5	1749.3	2.2	4.71	−0.18
0	1	2	34789.4	34828.2	5.22	0.370	34784.5	2335.5	2336.6	−1.0	4.42	0.81
1	1	0	34620.1	34656.4	4.91	0.370	34615.6	2166.6	2168.5	−1.9	5.07	−0.16
1	1	1	35197.1	35228.8	4.34	0.373	35193.1	2744.1	2741.9	2.2	4.78	−0.44

[a]Values in cm^{-1}.
[b]Uncertainty ± 0.2 cm^{-1}.
[c]Uncertainty ± 0.02 cm^{-1}.
[d]Uncertainty ± 0.001 cm^{-1}.
[e]Difference from the experimental value.

$$E_0+E'_v=E_0+(v_3+1/2)\omega_3+(v_4+1/2)\omega_4+(v_5+1/2)\omega_5 +(v_3+1/2)^2\chi_{33}+(v_4+1/2)^2\chi_{44}+(v_5+1/2)^2\chi_{55} +(v_3+1/2)(v_4+1/2)\chi_{34}+(v_3+1/2)(v_5+1/2)\chi_{35} +(v_4+1/2)(v_5+1/2)\chi_{45}-(\omega_3+\omega_4+\omega_5)/2 -(\chi_{33}+\chi_{44}+\chi_{55}+\chi_{34}+\chi_{35}+\chi_{45})/4, \quad (1)$$

where E_0 is the energy of the origin, ω_i is the harmonic frequency of each vibration, and χ_{ii} and χ_{ij} are the diagonal and off-diagonal anharmonicities, respectively. Similarly, we fit the observed A' rotational constants for each vibrational level to the usual expression,[37]

$$A'_v=A'_e-\alpha_3(v_3+1/2)-\alpha_4(v_4+1/2)-\alpha_5(v_5+1/2), \quad (2)$$

where A'_e is the equilibrium *a*-axis rotational constant and α_i is the vibration-rotation interaction constant. Table I gives all of the parameters for the fit, and the same parameters give the progressions that label the transitions in Figs. 4 and 5. Table II is a comparison of the calculated and measured line positions and rotational constants for the transitions from the origin up to 35 000 cm^{-1} that we used in the fit.

Even though the spectral congestion at higher energies makes the simultaneous fitting of those line positions difficult, we are able to assign the high energy $K'_a=1\leftarrow K''_a=0$ transitions using three criteria; the agreement with calculated line positions, the consistency of the frequencies in the assigned progressions, and the clear identification of strong and weak transitions with vibrations producing correspondingly large and small Franck–Condon factors. The parameters reported in Table I come from a nonlinear least-squares fit of the less congested, low energy portion of the spectrum with transitions listed in Table II. A separate fit including all of the $K'_a=1\leftarrow K''_a=0$ transitions up to 38 500 cm^{-1} produced a slightly different set of parameters that lie within the uncertainties of the fitting parameters for the low energy transitions (Table I). A small variation in the fit parameters is not surprising for the large frequency range covered with only three vibrational modes in the simulations. Transitions of three modes with harmonic frequencies of $\omega_3=1034$ cm^{-1}, $\omega_4=1192$ cm^{-1}, and $\omega_5=599$ cm^{-1} fit most of the strong progression in the region up to 38 000 cm^{-1} and many of those at energies up to 40 000 cm^{-1}. Table III gives the identities and wave numbers for the progressions whose assignments are secure.

B. Vibrational assignments

Confirming the identities of the motions associated with the frequencies of the three vibrational modes requires that we consider the geometry of the electronically excited state and the Franck–Condon factors for the transitions. Dixon and Kirby observed multiple 530–580 cm^{-1} progressions in their pioneering study of the ultraviolet absorption spectrum of HNCO.[2] They assigned the vibrational progressions to N–C–O bending motions built on various unassigned vibrations, a conclusion supported by their analysis of the rotational contours showing that the N–C–O moiety is bent in the excited state. We observe the progressions that they label B and C but do not find their A and D progressions, probably because the latter arise from thermally populated levels to which we are insensitive.

Several theoretical studies of the S_1 state of HNCO agree with their inference that the N–C–O bond angle decreases from 171° in S_0 to about 125° in S_1.[22,24,26,39,40] Calculations find both *cis* and *trans* isomers with the *trans* isomer lying about 1000–2000 cm^{-1} lower in energy than the *cis* isomer.[22,24,26] Stevens *et al.* calculate that the $S_1\leftarrow S_0$ transition dipole moment from the ground state nuclear configuration to the *trans* isomer in the excited state is more than ten times greater than that to the *cis* isomer.[24] The theoretical

TABLE III. Observed wave numbers and assignments for transitions to $K'_a=1$ states of S_1.

N–C stretch v_3	H–N–C bend v_4	N–C–O bend v_5	Wave number[a] (cm^{-1})	N–C stretch v_3	H–N–C bend v_4	N–C–O bend v_5	Wave number[a] (cm^{-1})
0	0	0		4	0	1	36877.8
0	0	1	33043.4	4	0	2	37425.2
0	0	2	33633.2	4	0	3	37972.8
0	0	3	34223.0	4	0	4	38516.4
0	0	4	34812.1				
0	0	5	35401.5	0	1	1	34204.6
0	0	6	35989.8	0	1	2	34789.4
0	0	7	36577.3	0	1	3	35373.2
0	0	8	37163.4	0	1	4	35954.1
0	0	9	37748.2				
0	0	10	38332.0	1	1	0	34620.1
				1	1	1	35197.1
1	0	0	33458.4	1	1	2	35776.7
1	0	1	34033.7	1	1	3	36356.7
1	0	2	34608.8	1	1	4	36935.7
1	0	3	35181.8	1	1	5	37515.7
1	0	4	35752.3	1	1	6	38094.7
1	0	5	36320.8				
1	0	6	36889.3	2	1	0	35593.5
1	0	7	37456.4	2	1	1	36160.8
1	0	8	38024.8	2	1	2	36725.8
1	0	9	38593.4	2	1	3	37288.0
				2	1	4	37847.4
2	0	0	34439.0	2	1	5	38399.8
2	0	1	35006.0				
2	0	2	35572.0	3	1	1	37101.8
2	0	3	36136.6	3	1	2	37659.1
2	0	4	36699.5	3	1	3	38213.3
2	0	5	37260.4	3	1	4	38763.4
2	0	6	37819.5	3	1	5	39308.0
2	0	7	38379.0				
				1	2	0	35752.3
3	0	0	35396.3	1	2	1	36333.5
3	0	1	35954.9	1	2	2	36911.3
3	0	2	36511.7	1	2	3	37482.1
3	0	3	37067.4	1	2	4	38051.1
3	0	4	37622.8				
3	0	5	38174.7	2	2	1	37304.2
3	0	6	38723.6	2	2	2	37875.5
				2	2	3	38444.4

[a]Uncertainty ± 0.5 cm^{-1}.

studies also find that the N–C bond length increases by about 0.2 Å while the H–N–C bond angle decreases by about 10° between the S_0 and S_1 states.[22,24,26,39] All of the theoretical calculations agree that the C–O and N–H bond lengths are about the same in the two electronic states.

We performed a series of calculations of the S_1 state geometry to help understand the vibrational modes and frequencies qualitatively. We used the GAUSSIAN 94W and 98W computational chemistry programs to calculate the optimized geometry and normal modes of the S_1 electronic state using configuration interaction-singles (CIS) with various basis sets up to 6-311++G(3*d*,2*p*).[41,42] Figure 6 shows the resulting normal modes of the *trans* isomer of S_1 calculated at that level, with the vibrational frequencies scaled by 0.9 to compensate for systematic errors in the level of theory.[43] We label the normal modes to emphasize their similarities with the normal modes of S_0. Our designation follows the convention recommended by Mulliken[44] except in the case of the H–N–C bending motion, ν_4, and the N–C stretching motion, ν_3, in that the first lies higher in energy but receives the larger number. The *cis* isomer vibrations are similar to those of the *trans* isomer in both frequency and character.

Table IV gives our experimental and several calculated electronic energies and vibrational frequencies. They all predict a N–C–O bending frequency between 560 cm^{-1} and 605 cm^{-1}, consistent with the lower frequency progression in the experimental spectra. There are no other vibrations with similar frequencies, and the calculations support Dixon and Kirby's assignment of the progressions to the N–C–O bending vibrations built on various other vibrational motions.[2] The calculations predict a N–C stretching frequency in the range of 875 cm^{-1} to 1080 cm^{-1} and a H–N–C bending frequency in the range of 1055 cm^{-1} to 1220 cm^{-1}, both reasonably close to the values that fit our observed progressions. The calculated geometry changes strongly suggest that the N–C stretching vibration is respon-

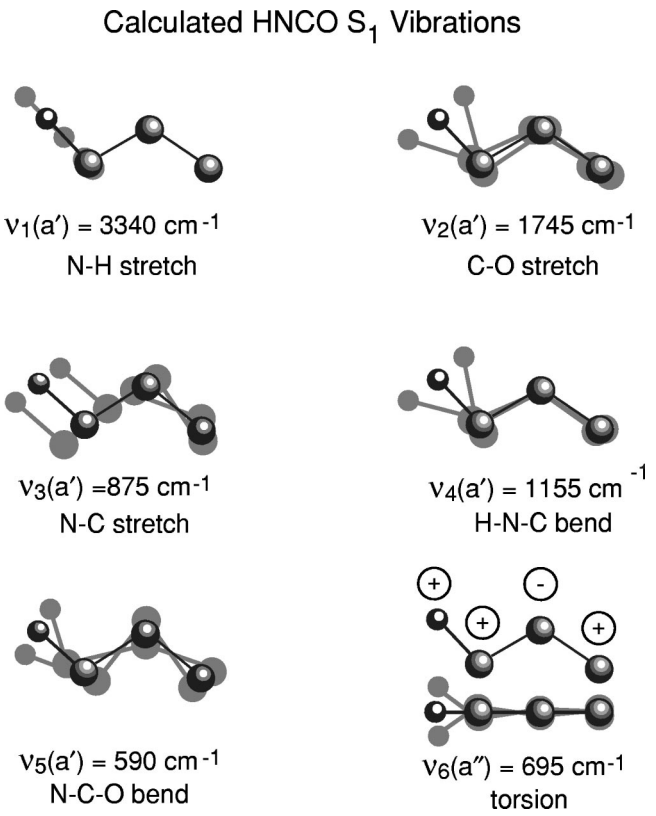

FIG. 6. Calculated normal modes and frequencies for vibrations in the first electronically excited state of HNCO. The labels give the dominant motion in the normal mode.

sible for the relatively long 1034 cm^{-1} progression since electronic excitation from S_0 to S_1 increases the N–C bond length by almost 0.2 Å, a change that produces transitions to levels with at least four quanta of the stretching vibration. Because electronic excitation changes the H–N–C bond angle by only about 10°, the H–N–C bend is the more likely candidate for the 1192 cm^{-1} mode that appears with only one or two quanta of excitation.

Assigning other modes from weak transitions observed in our spectra is very speculative, but the quality of the agreement between the calculated and measured frequencies for the three modes we assign indicates that the calculations are a useful guide. For example, we observe a weak feature at 34 233 cm^{-1}, 1784 cm^{-1} above the proposed origin, that is consistent with the calculated frequency of the C–O stretch (ν_2) given in Table IV, and, although the congestion at higher levels makes the process uncertain, we even identify a few candidates for N–C–O bending (ν_5) progressions built on a combination of the C–O and N–C stretching ($\nu_2+\nu_3$). Table III summarizes our assignment of strong bands to combinations of the N–C stretching (ν_3), the H–N–C bending (ν_4), and the N–C–O bending (ν_5) vibrations, consistent with our qualitative analysis of the Franck–Condon factors.

C. Origin of S_1

The lowest energy transition we observe is a rigorous upper limit to the energy of the origin of the first excited singlet state in HNCO, and the fit to the progressions suggests that the origin actually lies one vibrational quantum below that lowest energy transition. As Fig. 5 and Table I show, we build the simulation on a common level at 32 449±20 cm^{-1}, which is our best estimate of the origin of the S_1 electronic state. There might be still lower lying states that we do not detect because transition probabilities to them, even from the vibrationally excited state we prepare, are too small, but the simplicity of the progressions at the lowest energies argues against a lower S_1 origin. If the vibrational level at 32 499±20 cm^{-1} is not the S_1 origin, it must be a state that dramatically improves the photofragment yield of vibrational levels built on it. Otherwise we would see transitions to many more states and would observe several progressions built on different, lower lying vibrations in the region from 33 000 to 35 000 cm^{-1}. The three calculations summarized in Table IV give values of 32 970 cm^{-1}, 31 600 cm^{-1}, and 30 600 cm^{-1} for the origin. The first[26] exceeds our estimate by less than 500 cm^{-1}, and the second[23] lies about 900 cm^{-1} below our estimate, amounts that are close to the probable uncertainty in the calculations.

D. Radiationless decay of S_1

The variation in the linewidths in NCO and NH photofragment yield spectra of HNCO suggests that certain modes promote the internal conversion from S_1 to S_0.[20,21] With the assignment of several of the vibrations of S_1 in hand, we can

TABLE IV. Experimental and calculated energies and harmonic vibrational frequencies of HNCO(S_1).[a]

		Calculation[b]			
	Experiment	This work	Stanton[c]	Schinke[d]	Morokuma[e]
E_0	32 449±20		32 970	31 500	30 600
ν_1 (N–H stretch)		3340	3495		3510
ν_2 (C–O stretch)		1745	1735		1800
ν_3 (N–C stretch)	1034±11	875	1080	915	960
ν_4 (H–N–C bend)	1192±19	1155	1220		1055
ν_5 (N–C–O bend)	599±7	590	605	595	560
ν_6 (torsion)		695	715		

[a]Values in cm^{-1}.
[b]Calculated values reported to the nearest 5 cm^{-1}.
[c]Reference 26.
[d]Reference 23.
[e]References 18 and 25.

identify a promoting mode for internal conversion. The rotational contours of nearby bands in a jet-cooled sample (Fig. 2 of Ref. 21) show that the linewidth changes substantially with the vibrational mode excited. Two features at 36 578 cm^{-1} and 37 164 cm^{-1} have well-resolved rotational structure, but line broadening obscures the rotational structure of another feature that lies between the two at 37 068 cm^{-1}. Our vibrational assignments in Table III identify the two sharp features as transitions to pure bending states with seven $(7\nu_5)$ and eight $(8\nu_5)$ quanta of N–C–O bending excitation, respectively. In contrast, the broader feature is a transition to a state with three quanta each of N–C stretching and N–C–O bending excitation $(3\nu_3,3\nu_5)$. The N–C stretching excitation appears to shorten the lifetime of the excited state, and the comparison suggests that it is a promoting mode for internal conversion from S_1 to S_0. Similar comparisons[20] with other bands that include multiple quanta of ν_3 excitation lead to the same conclusion.

V. SUMMARY

Vibrationally mediated photofragment yield spectroscopy is a powerful tool for examining low lying vibrational levels of excited electronic states whose equilibrium geometries differ significantly from the ground electronic state, and multiphoton fluorescence spectroscopy of molecules cooled in a supersonic expansion gives access to a broad range of states at slightly higher energies. Using these two approaches, we observe vibrational levels of the first excited singlet state of HNCO at energies from 33 000 cm^{-1} to 38 500 cm^{-1}. Fitting the sparse spectra at the lowest energies locates the origin of S_1 at $32\,449 \pm 20\ cm^{-1}$ and identifies progressions involving N–C stretching vibrations ($\omega_3 = 1034 \pm 11\ cm^{-1}$), H–N–C bending vibrations ($\omega_4 = 1192 \pm 19\ cm^{-1}$) and N–C–O bending vibrations ($\omega_5 = 599 \pm 7\ cm^{-1}$). The activity of the N–C–O bending and the N–C stretching vibrations in the spectra is consistent with the changes in N–C–O bond angle and the N–C bond length in going from S_0 to S_1, and the simplicity of the spectroscopy in the 33 000 cm^{-1} to 35 000 cm^{-1} region is consistent with levels in that region being near the spectroscopic origin of S_1. Identification of these vibrational modes in S_1 allows us to assign most of the strong progressions up to 40 000 cm^{-1} in the spectrum and to propose that the N–C stretching vibration promotes internal conversion from S_1 to S_0.

ACKNOWLEDGMENTS

We gratefully acknowledge the support of this work at both the University of Wisconsin-Madison and at the University of Southern California by the Division of Chemical Sciences of the Office of Basic Energy Sciences of the Department of Energy. We appreciate helpful discussions and communication of results prior to publication by Professor K. Morokuma, Dr. R. Schinke, and Professor J. F. Stanton. We thank Professor R. A. Beaudet and Ms. Lin Feng for their help in fitting the spectra.

[1] R. A. Perry and D. L. Siebers, Nature (London) **324**, 657 (1986); J. A. Canton and D. L. Siebers, Combust. Sci. Technol. **65**, 277 (1989).
[2] R. N. Dixon and G. H. Kirby, Trans. Faraday Soc. **64**, 2002 (1968).
[3] K. Yamada, J. Mol. Spectrosc. **79**, 323 (1980).
[4] B. Lemoine, K. Yamada, and G. Winnewisser, Ber. Bunsenges. Phys. Chem. **86**, 795 (1982).
[5] G. Herzberg and C. Reid, Discuss. Faraday Soc. **9**, 92 (1950).
[6] D. A. Steiner, S. R. Polo, and J. T. K. McCubbin, J. Mol. Spectrosc. **98**, 453 (1983).
[7] D. A. Steiner, K. A. Wishah, S. R. Polo, and T. K. McCubbin, J. Mol. Spectrosc. **76**, 341 (1979).
[8] L. Fusina, M. Carlotti, and B. Carli, Can. J. Phys. **62**, 1452 (1984).
[9] M. Niedenhoff, K. M. T. Yamada, G. Winnewisser, and S. C. Ross, J. Mol. Struct. **352**, 423 (1995).
[10] M. Niedenhoff, K. M. T. Yamada, S. P. Belov, and G. Winnewisser, J. Mol. Spectrosc. **174**, 151 (1995).
[11] M. Niedenhoff, K. M. T. Yamada, and G. Winnewisser, J. Mol. Spectrosc. **176**, 342 (1996).
[12] A. L. L. East, C. S. Johnson, and W. D. Allen, J. Chem. Phys. **98**, 1299 (1993).
[13] N. Pinnavaia, M. J. Bramley, M. D. Su, W. H. Green, and N. C. Handy, Mol. Phys. **78**, 319 (1993).
[14] A. M. Mebel, A. Luna, M. C. Lin, and K. Morokuma, J. Chem. Phys. **105**, 6439 (1996).
[15] K. Yokoyama, S. Takane, and T. Fueno, Bull. Chem. Soc. Jpn. **64**, 2230 (1991).
[16] S.-C. Woo and T.-K. Liu, J. Chem. Phys. **3**, 544 (1935).
[17] M. Zyrianov, Th. Droz-Georget, and H. Reisler, J. Chem. Phys. **110**, 2059 (1999).
[18] A. L. Kaledin, Q. Cui, M. C. Heaven, and K. Morokuma, J. Chem. Phys. **111**, 5004 (1999).
[19] M. Zyrianov, Th. Droz-Georget, A. Sanov, and H. Reisler, J. Chem. Phys. **110**, 10774 (1999).
[20] M. Zyrianov, Th. Droz-Georget, A. Sanov, and H. Reisler, J. Chem. Phys. **105**, 8111 (1996).
[21] M. Zyrianov, Th. Droz-Georget, and H. Reisler, J. Chem. Phys. **106**, 7454 (1997).
[22] J. J. Klossika, H. Flothmann, C. Beck, R. Schinke, and K. Yamashita, Chem. Phys. Lett. **276**, 325 (1997).
[23] J. J. Klossika and R. Schinke, J. Chem. Phys. **111**, 5882 (1999).
[24] J. E. Stevens, Q. Cui, and K. Morokuma, J. Chem. Phys. **108**, 1452 (1998).
[25] A. Kaledin and K. Morokuma (personal communication, 1999).
[26] J. F. Stanton (personal communication, 1998). The calculations optimized ground and excited state geometries with a double-zeta plus polarization basis set using coupled-cluster theory in the singles and doubles approximation (CCSD) for S_0 and the corresponding equation-of-motion technique for the S_1 states. See, J. F. Stanton and R. J. Bartlett, J. Chem. Phys. **98**, 7029 (1993); J. F. Stanton, *ibid.* **99**, 8840 (1993); O. Christiansen, H. Koch, and P. Jørgensen, *ibid.* **103**, 7429 (1995) for a discussion of the quantum chemical methods used.
[27] D. S. King, P. K. Schenck, K. C. Smyth, and J. C. Travis, Appl. Opt. **16**, 2617 (1977); K. C. Smyth and P. K. Schenck, Chem. Phys. Lett. **55**, 466 (1978).
[28] R. N. Dixon, Can. J. Phys. **37**, 1171 (1959).
[29] C. R. Brazier, R. S. Ram, and P. F. Bernath, J. Mol. Spectrosc. **120**, 381 (1986).
[30] W. Ubachs, J. J. ter Meulen, and A. Dymanus, Can. J. Phys. **62**, 1374 (1984).
[31] R. A. Ashby and R. L. Werner, J. Mol. Spectrosc. **18**, 184 (1965).
[32] S. S. Brown, H. L. Berghout, and F. F. Crim, J. Chem. Phys. **102**, 8440 (1995).
[33] K. Uno, T. Hikida, A. Hiraya, and K. Shobatake, Chem. Phys. Lett. **166**, 475 (1990).
[34] K. M. T. Yamada, M. Winnewisser, and J. W. C. Johns, J. Mol. Spectrosc. **140**, 353 (1990).
[35] S. S. L. Brown, Ph.D. thesis, University of Wisconsin-Madison, 1996.
[36] S. S. Brown, H. L. Berghout, and F. F. Crim, J. Chem. Phys. **106**, 5805 (1997).
[37] I. N. Levine, *Molecular Spectroscopy* (Wiley, New York, 1975).
[38] E. B. Wilson, *Molecular Vibrations: The Theory of Infrared and Raman Vibrational Spectra* (McGraw–Hill, New York, 1955).
[39] S. S. Brown, C. M. Cheatum, D. A. Fitzwater, and F. F. Crim, J. Chem. Phys. **105**, 10911 (1996).
[40] The transition intensities increase roughly in proportion to the number of vibrational quanta for wave numbers up to 35 000 cm^{-1}, and we arbitrarily scale the intensity of each transition in the simulation linearly with the

number of vibrational quanta contained in the N–C stretch and the N–C–O bend as $I=I_0+I_3v_3+I_4v_4+I_5v_5$.

[41] M. J. Frisch, G. W. Trucks, H. B. Schlegel, P. M. W. Gill, B. G. Johnson, M. A. Robb, J. R. Cheeseman, T. Keith, G. A. Petersson, J. A. Montgomery, K. Raghavachari, M. A. Al-Laham, V. G. Zakrzewski, J. V. Ortiz, J. B. Foresman, J. Cioslowski, B. B. Stefanov, A. Nanayakkara, M. Challacombe, C. Y. Peng, P. Y. Ayala, W. Chen, M. W. Wong, J. L. Andres, E. S. Replogle, R. Gomperts, R. L. Martin, D. J. Fox, J. S. Binkley, D. J. Defrees, J. Baker, J. P. Stewart, M. Head-Gordon, C. Gonzalez, and J. A. Pople, GAUSSIAN 94W, Revision E.3, Gaussian, Inc., Pittsburgh, Pennsylvania, 1995.

[42] M. J. Frisch, G. W. Trucks, H. B. Schlegel, G. E. Scuseria, M. A. Robb, J. R. Cheeseman, V. G. Zakrzewski, J. J. A. Montgomery, R. E. Stratmann, J. C. Burant, S. Dapprich, J. M. Millam, A. D. Daniels, K. N. Kudin, M. C. Strain, O. Farkas, J. Tomasi, V. Barone, M. Cossi, R. Cammi, B. Mennucci, C. Pomelli, C. Adamo, S. Clifford, J. Ochterski, G. A. Petersson, P. Y. Ayala, Q. Cui, K. Morokuma, D. K. Malick, A. D. Rabuck, K. Raghavachari, J. B. Foresman, J. Cioslowski, J. V. Ortiz, B. B. Stefanov, G. Liu, A. Liashenko, P. Piskorz, I. Komaromi, R. Gomperts, R. L. Martin, D. J. Fox, T. Keith, M. A. Al-Laham, C. Y. Peng, A. Nanayakkara, C. Gonzalez, M. Challacombe, P. M. W. Gill, B. Johnson, W. Chen, M. W. Wong, J. L. Andres, C. Gonzalez, M. Head-Gordon, E. S. Replogle, and J. A. Pople, GAUSSIAN 98W, Revision A.3, Gaussian, Inc., Pittsburgh, Pennsylvania, 1998.

[43] J. B. Foresman, A. Frisch, and I. Gaussian, *Exploring Chemistry with Electronic Structure Methods*, 2nd ed. (Gaussian Inc., Pittsburgh, PA, 1996).

[44] R. S. Mulliken, J. Chem. Phys. **23**, 1997 (1955).